Supplementary Information (SI) for Journal of Materials Chemistry C.
This journal is © The Royal Society of Chemistry 2026

Interpretable machine learning-assisted discovery of Ba-TiO_3-based ceramics with enhanced dielectric constant

Jian Liu, Hua Hao*, Xingzhong Liu, Jiahao Tian, Bangzhi Peng, Chunze Wei, Jinglong Fan, Hanxing Liu*

State Key Laboratory of Advanced Technology for Materials Synthesis and Processing, School of Material Science and Engineering, International School of Material Science and Engineering, Wuhan University of Technology, Wuhan, 430070, China

*Corresponding authors:

E-mail: haohua@whut.edu.cn, lhxhp@whut.edu.cn

Table S1 Detailed list of initial features

Feature	Description
AN	Atomic number of A-site, B-site element in periodic table
AM	Relative atomic mass of A-site, B-site element
AV	Atomic volume of A-site, B-site element
AD	Atomic density of A-site, B-site element
PE	Period of A-site, B-site element in periodic table
Group	Group of A-site, B-site element in periodic table
MN	Mendeleev number of A-site, B-site element [1]
IR	Shannon's ionic radius of A-site, B-site element [2]
AR	Atomic radius of A-site, B-site element [3]
VR	van der Waals radius of A-site, B-site element[4]
CR	Covalent radius of A-site, B-site element [5]
PR	Pseudopotential core radius of A-site, B-site element [6]
BDP	Ideal A–O, B–O bond distance [7]
DC	Core electron distance (Schubert) of A-site, B-site element [8]
DV	Valence electron distance (Schubert) of A-site, B-site element [8]
EFF_C	Effective nuclear charge (Clementi) of A-site, B-site element [8]

EFF_S	Effective nuclear charge (Slater) of A-site, B-site element [9]
DP	Static average electric dipole polarizability of A-site, B-site element [10]
EP	Empirical electronic polarizability of A-site, B-site element[11]
z_ir	Ratio of nominal charge to Shannon's ionic radius of A-site, B-site element
EA	Electron affinity of A-site, B-site element [8]
EI_F	First ionization energy of A-site, B-site element [8]
EI_S	Second ionization energy of A-site, B-site element [8]
EN_P	Electronegativity (Pauling scale) of A-site, B-site element [8]
EN_B	Electronegativity (Martynov–Batsanov) of A-site, B-site element [8]
EN_T	Electronegativity (Thermochemical) of A-site, B-site element[12]
NUM_S	Number of electrons in the s orbital of A-site, B-site element
NUM_P	Number of electrons in the p orbital of A-site, B-site element
NUM_D	Number of electrons in the d orbital of A-site, B-site element
NUM_F	Number of electrons in the f orbital of A-site, B-site element
t	Tolerance factor calculated by Shannon's ionic radius

Table S2 Comparison of 10-fold cross-validation R^2 over 100 repetitions for the top four performing algorithmic models

Algorithm	Maximum	Average
ETR	0.890	0.875
GBR	0.864	0.850
LGBM	0.863	0.848
XGB	0.851	0.834

Table S3 Comparison of mean R^2 values from 100 times of 10-fold cross-validation across feature subsets of various dimensions

Feature subset dimension	61	26	11	6
Mean R^2	0.875	0.877	0.873	0.874

Table S4 The chemical elements occupying the A-site and B-site

A-site	Ba	Ca	La	Sr	Dy								
B-site	Ti	Mg	Nb	Zr	Zn	Sn	Ta	Y	Ni	Fe	Hf	W	Yb	Co

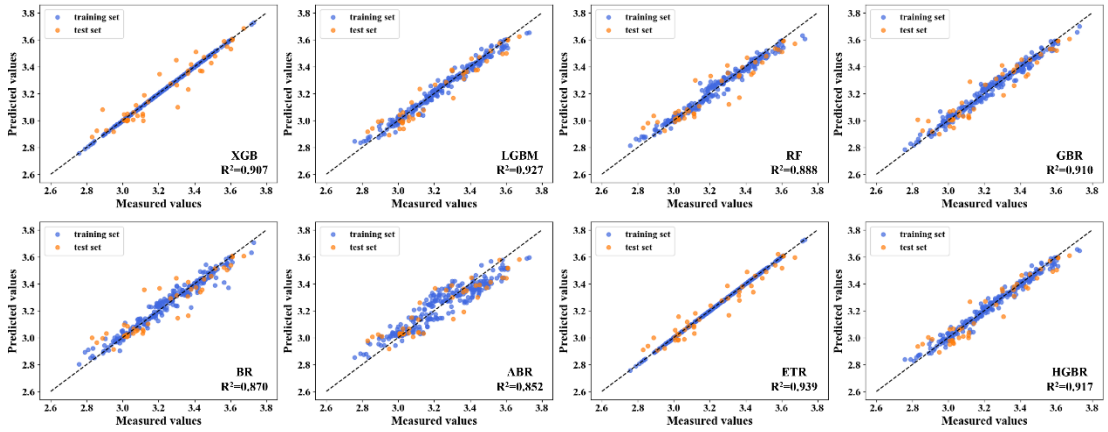

Fig. S1 Comparison of predicted and measured values for dielectric constant.

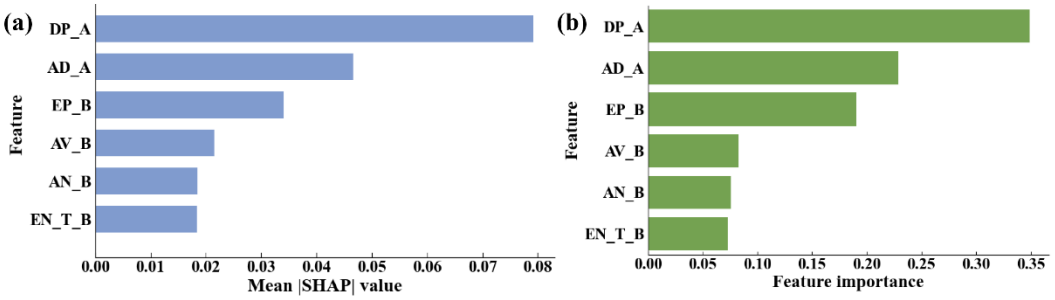

Fig. S2 Feature importance rankings of the optimal feature subset obtained by (a) SHAP analysis and (b) ETR model.

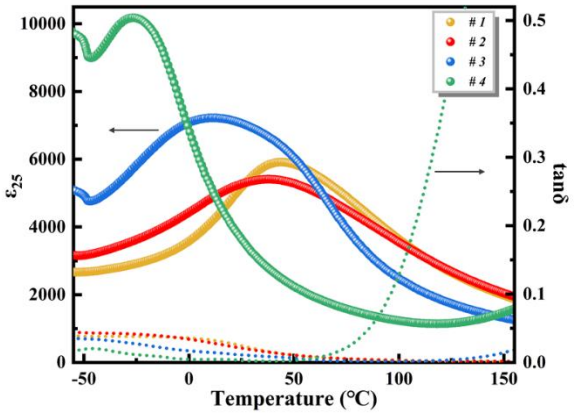

Fig. S3 Dielectric constant and dielectric loss as a function of temperature at 1 kHz for four newly synthesized compositions

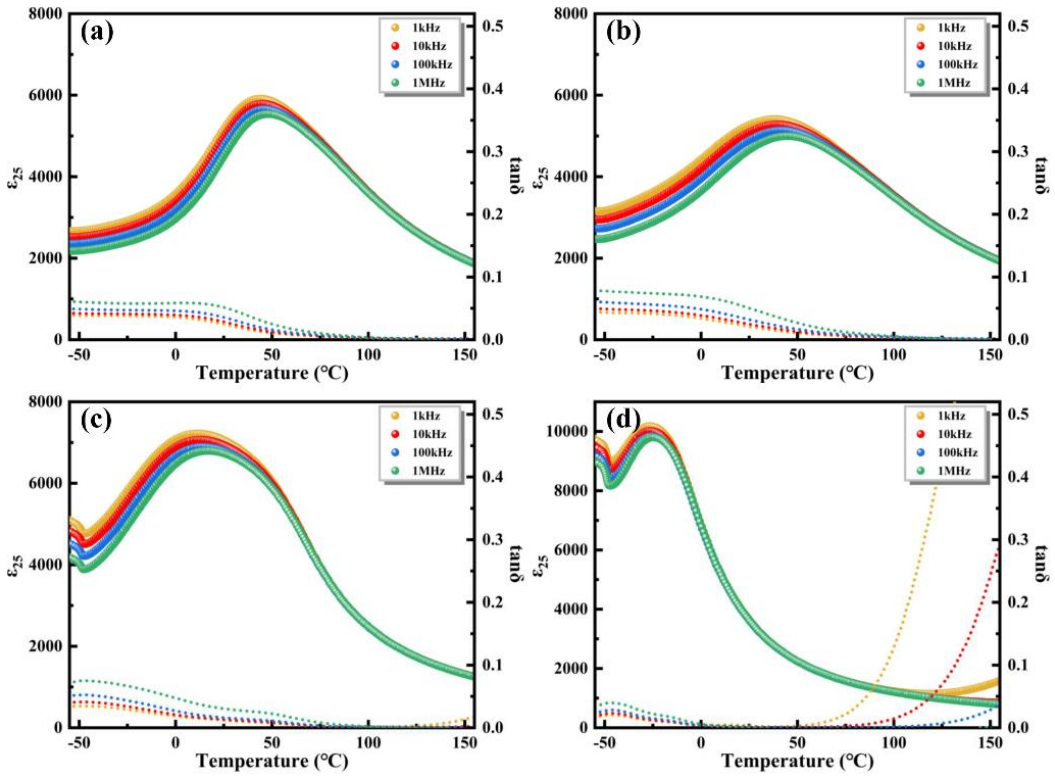

Fig. S4 Temperature dependence of dielectric properties at various measurement frequencies for the four newly synthesized compositions (a) #1; (b) #2; (c) #3; (d) #4.

Experimental details

The four newly synthesized compounds were prepared by solid-state reaction method. First, the raw materials were weighed according to the stoichiometric ratios using an electronic balance and then transferred into the ball mill jar. An appropriate amount of anhydrous ethanol and zirconia balls were added, and the mixture was ball-

milled for 4 hours. The resulting slurry was dried in an oven, and the dried powder was ground and then pre-calcined at 1150 °C. After pre-calcination, the powder was subjected to a second ball-milling, and followed by drying process. Subsequently, 5 wt.% PVA was added as a binder to the dried powder for granulation, and the granulated powder was then uniaxially dry-pressed into green pellets (≈12 mm in diameter, ≈1 mm in thickness). The green pellets were subjected to binder removal in a muffle furnace at 600 °C for 2 h, followed by sintering at 1320~1400 °C. Prior to electrical measurements, both sides of the sintered samples were polished and coated with silver paste. After a subsequent calcination step, silver electrodes were formed on the surfaces, thereby constructing a capacitor structure for further testing. The dielectric properties were measured over a frequency range of 10^3~10^6 Hz.

References

1 P. Villars, K. Cenzual, J. Daams, Y. Chen and S. Iwata, *J. Alloys Compd.*, 2004, **367**, 167–175.

2 R.D.Shannon, *Acta Cryst*, 1976, **32**, 751–767.

3 J.C. Slater, *J. Chem. Phys.*, 1964, **41**, 3199–3204.

4 S. S. Batsanov, *Inorganic Materials*, 2001, **37**, 871–885.

5 B. Cordero, V. Gómez, A. E. Platero-Prats, M. Revés, J. Echeverría, E. Cremades, F. Barragán and S. Alvarez, *Dalton Transactions*, 2008, 2832–2838.

6 A. Zunger, *Phys. Rev. B*, 1980, **22**, 5839–5872.

7 N. E. Brese and M. O'keeffe, *Acta Cryst*, 1991, **47**, 192–197.

8 https://www.webelements.com.

9 J. C. Slater, *physical review*, 1930, **36**, 57–64.

10 D.R. Lide, H. William M, CRC handbook of chemistry and physics: A ready-reference book of chemical and physical data, CRC, Boca Raton, FL, USA, 2004

11 R. D. Shannon and R. X. Fischer, *Phys. Rev. B*, 2006, **73**, 235111.

12 C. Tantardini and A. R. Oganov, *Nat. Commun.*, 2021, **12**, 2087.